17

Integrated Planetary Geoscience: A Case Study (Mars)

Planetary exploration typically advances in step with technology. Improvements in spatial and spectral resolution yield discoveries that progress from global to regional scales, and exploration on a planet's surface provides ground truth for remote sensing data and a level of observation and measurement that geologists crave. Samples that can be analyzed in the laboratory provide geochemical and geochronologic information that complements spacecraft data and enhances its interpretation. We illustrate how data at all these scales have been integrated to characterize the complex geology of Mars and to constrain its geologic history.

17.1 Geologic Exploration of a Planet

Planetary geologic exploration normally progresses in stages, from global reconnaissance to regional investigations, and thence to local mapping and analysis. The first stage is begun using ground-based telescopes and flyby or orbiting spacecraft, the second stage utilizes orbiters, and the third focuses on landed spacecraft and rovers. These stages are not always strictly sequential, but changes in the spatial scale of investigation normally happen in step with improvements in technology over time. This progression is opposite to the strategy of terrestrial geologists, where local studies are combined and synthesized to understand the Earth at regional and then global scales. In this chapter we will see examples of how planetary geology is done at each of these scales.

We focus here on Mars, because it is the only planet, besides our own, that has progressed through all three stages of exploration. The Moon has also gone through these stages, with the added benefit of samples returned by astronauts. For the foreseeable future, though, exploration on the surfaces of other worlds will be accomplished robotically, which is the way Mars has been studied.

All the stages of planetary exploration utilize information familiar to terrestrial geologists – maps, topography, stratigraphy, geochronology, geomorphology, geophysics, geochemistry, mineralogy, and petrography. How these data are acquired may differ, but the strategies and principles of geologic exploration are the same.

The laboratory analysis of samples, whether returned or acquired as meteorites, provides a level of petrologic, geochemical, and geochronologic information that is otherwise unobtainable. The value of a sample is magnified if its specific provenance is known or can be determined.

17.2 Planetary Reconnaissance and a Global Geologic Map

Geologic understanding involves the integration of data at all spatial scales. This is usually done continuously. In the following, we consider the insights derived from global reconnaissance, and then illustrate studies of the regional and local geology of a few areas that have been explored by rovers. Then we add the insights gained from martian meteorites. Finally, we utilize all these data to synthesize the geologic history of Mars.

17.2.1 Global Physiography and Structure

The average thickness of the martian crust, as constrained by orbital gravity and topography measurements, is ~50 km, comprising as much as ~6 wt% of the silicate fraction (mantle plus crust) of Mars. The bulk density and moment of inertia factor are consistent with a core comprising ~22 wt% of the planet.

The most notable surface feature in orbital imagery is a global dichotomy that separates terrains that differ in topography, age, and crustal thickness. South of this boundary are the highlands – ancient, heavily cratered units with elevations higher than the global average.

Within the highlands are huge impact basins and magnetic lineations discovered by an orbiting magnetometer. To the north of the dichotomy are the lowlands – younger plains of layered sedimentary and volcanic rocks covering an ancient basement.

Magmatic centers (Tharsis, Elysium, Syrtis Major, Hesperia) host enormous volcanoes and vast outpourings of lavas. Martian tectonics are dominated by the Tharsis uplift, which is surrounded by a moat, radial rifts, concentric ridges, and a system of gigantic canyons.

Superimposed on both highlands and lowlands are layered sedimentary deposits. The accommodation of sediments on Mars is provided by water depth, rather than subsidence as on Earth, with the consequence that the stratigraphic record is discontinuous and is dominated by sediments produced by erosion. A pervasive regolith covers the surface. Polar caps are composed of interlayered ices and dust; the caps exchange icy materials annually and are the most dynamic regions of present-day Mars.

17.2.2 Global Remote Sensing

Orbiters have provided a number of global geoscience datasets. The acronyms are dizzying, and so are summarized below.

- *Mars Global Surveyor* (MGS, 1996–2006) carried a camera (MOC) for imagery, laser altimeter (MOLA) for topographic mapping, and thermal emission spectrometer (TES) for mineral identification; a magnetometer and radio science tracking discovered an ancient magnetic field and allowed the construction of a gravity map.
- *Mars Odyssey* (MO, 2001–present) featured a gamma ray/neutron spectrometer (GRS/NS) for geochemistry and a visible and thermal emission imager (THEMIS) for mineral mapping.
- ESA's *Mars Express* (MEx, 2003–present) operated an imager (HRSC) and a visible/near-infrared spectrometer (OMEGA) for mineral mapping.
- *Mars Reconnaissance Orbiter* (MRO, 2005–present) carried a high-resolution camera (HiRISE), an imaging spectrometer (CRISM) for mineralogy, and ground-penetrating radar (SHARAD).
- *Mars Atmosphere and Volatile Evolution* mission (MAVEN, 2013–present) features instruments designed to analyze the atmosphere to ascertain how Mars lost its water and atmosphere over time.
- *ExoMars Trace Gas Orbiter* (TGO, 2016–present) carries instruments to search for methane and other atmospheric gases that could be signatures of biologic or geologic processes; it also features an ultraviolet/infrared spectrometer (NOMAD) and a neutron detector (FREND) for sensing hydrogen.

The "global" datasets – albedo, topography, thermal inertia, gravity, magnetics, mineralogy (usually one mineral at a time, as shown in Figure 15.8), and geochemistry (only a handful of elements) – were actually obtained at regional scales and then combined to produce global maps. Some examples are illustrated in Figure 17.1.

17.2.3 Global Stratigraphic Timescale and Geologic Map

The observed geologic units on Mars are divided into the Noachian, Hesperian, and Amazonian systems, defined by stratigraphy and crater density measurements. As described in Section 15.3, mineralogical changes accompanying these periods are interpreted to reflect global environmental changes. The first approximately half-billion years of martian history (Pre-Noachian time) are not represented in the currently recognized rock record.

The most recent global geologic map of Mars (Figure 17.2; Tanaka et al., 2014) recognizes 44 geologic units. The map is based primarily on topography and imagery, which allow unit morphologies, stratigraphic relationships, and crater size–frequency data to be defined. Most of the surface of Mars is old, with Noachian units comprising 45 percent, Hesperian units 29 percent, and Amazonian units 26 percent of the planet's total surface.

17.3 Regional Geology from Orbit and Surface Exploration by Rovers

Although many interesting regions on Mars have been studied using multiple datasets as described above, we can only introduce a few. We will illustrate regional and local studies by focusing on three regions that have been studied from orbital spacecraft and subsequently explored from the ground. In these regions, rovers have conducted extensive traverses, providing more representative ground truth than provided by the *Viking* and *Phoenix* stationary landers or the very limited traverse of the *Mars Pathfinder* rover.

17.3.1 Gusev Crater

Orbital Studies

Gusev crater (~165 km diameter) is Noachian in age, but the deposits on its floor formed at ~650 Ma, based on crater counting data (Parker et al., 2010). Gusev was originally thought to be an ancient lakebed, based in part on the drainage of Ma'adim Vallis into it (Figure 17.3). Where the valley enters Gusev are flat-topped hills interpreted to be delta deposits. Using *Viking* orbiter imagery, a number of authors – most recently Kuzmin et al.

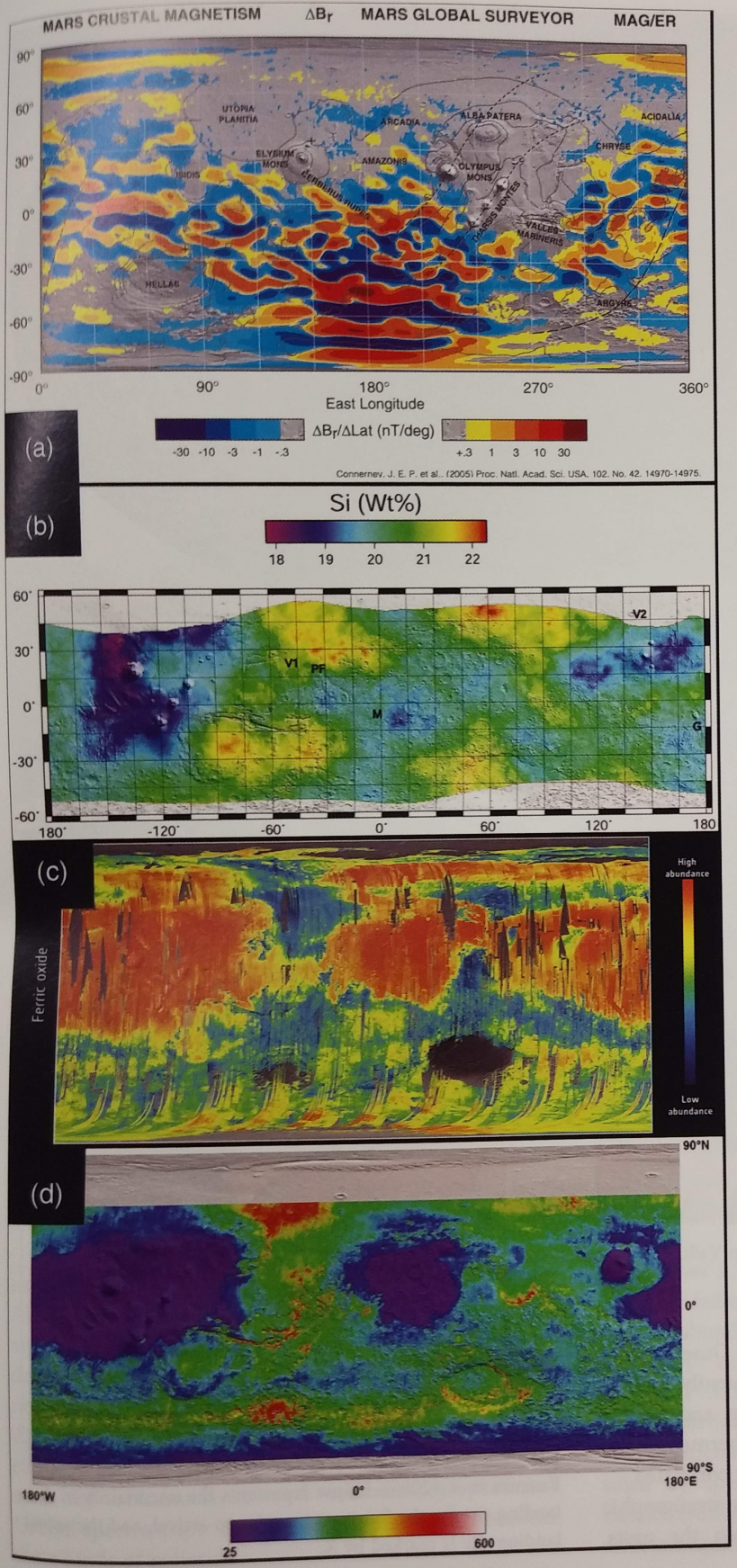

Figure 17.1 Examples of global maps of Mars obtained by orbiter instruments. (a) Magnetic field observed by MAG/ER on *Mars Global Surveyor* (Acuna et al., 2008). (b) Silicon abundance by GRS on *Mars Odyssey* (Boynton et al., 2008). (c) Abundance of crystalline ferric oxides by OMEGA on *Mars Express* (Bibring and Langevin, 2008). (d) Thermal inertia by THEMIS on *Mars Odyssey* (Christensen et al., 2008). Reprinted with permission from Cambridge University Press: The Martian Surface: Composition, Mineralogy, and Physical Properties, ed. J.F. Bell III, copyright (2008).

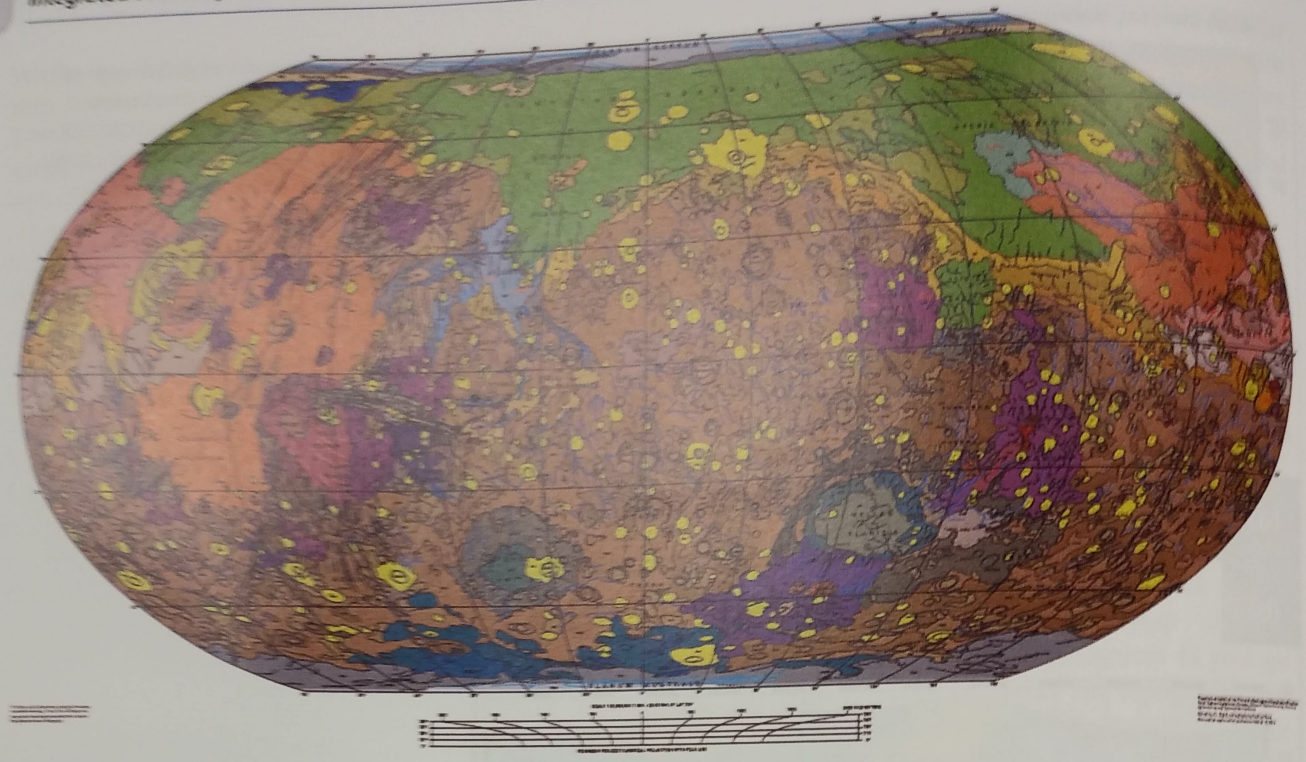

Figure 17.2 Global geologic map of Mars (US Geological Survey). See Tanaka et al. (2014) for explanation of units.

Figure 17.3 Image of Gusev crater and Ma'adim Vallis. NASA image.

(2000) – produced geologic maps of the Gusev region (Figure 17.4). Milam et al. (2003) subsequently utilized MOC imagery, THEMIS thermal mapping, and MOLA elevation data to identify and map seven thermophysical and morphologic units, which were largely correlated.

The existence of so many distinguishable stratigraphic units, as well as observed layering within the units,

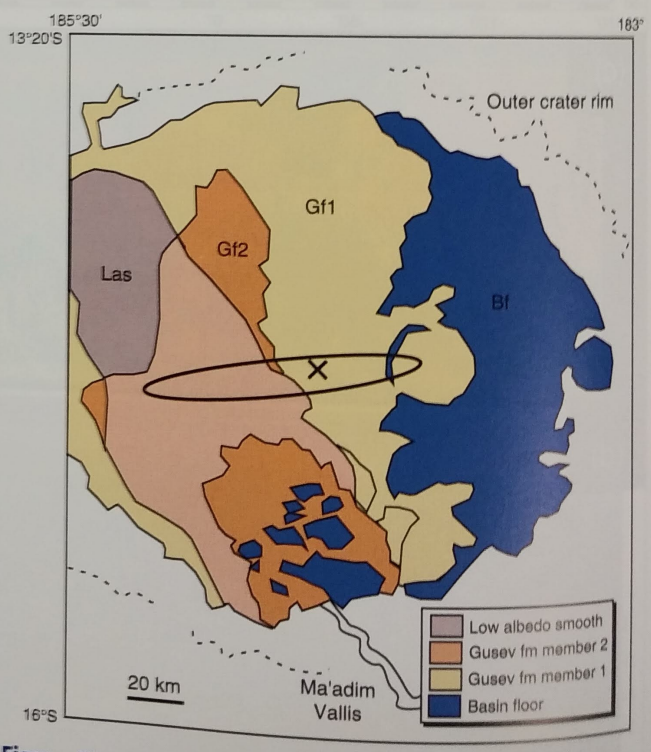

Figure 17.4 Geologic map of Gusev crater, simplified from Kuzmin et al. (2000). Ellipse represents the uncertainty in the landing site for the Spirit rover, prior to arrival, and the actual landing site is marked by X.

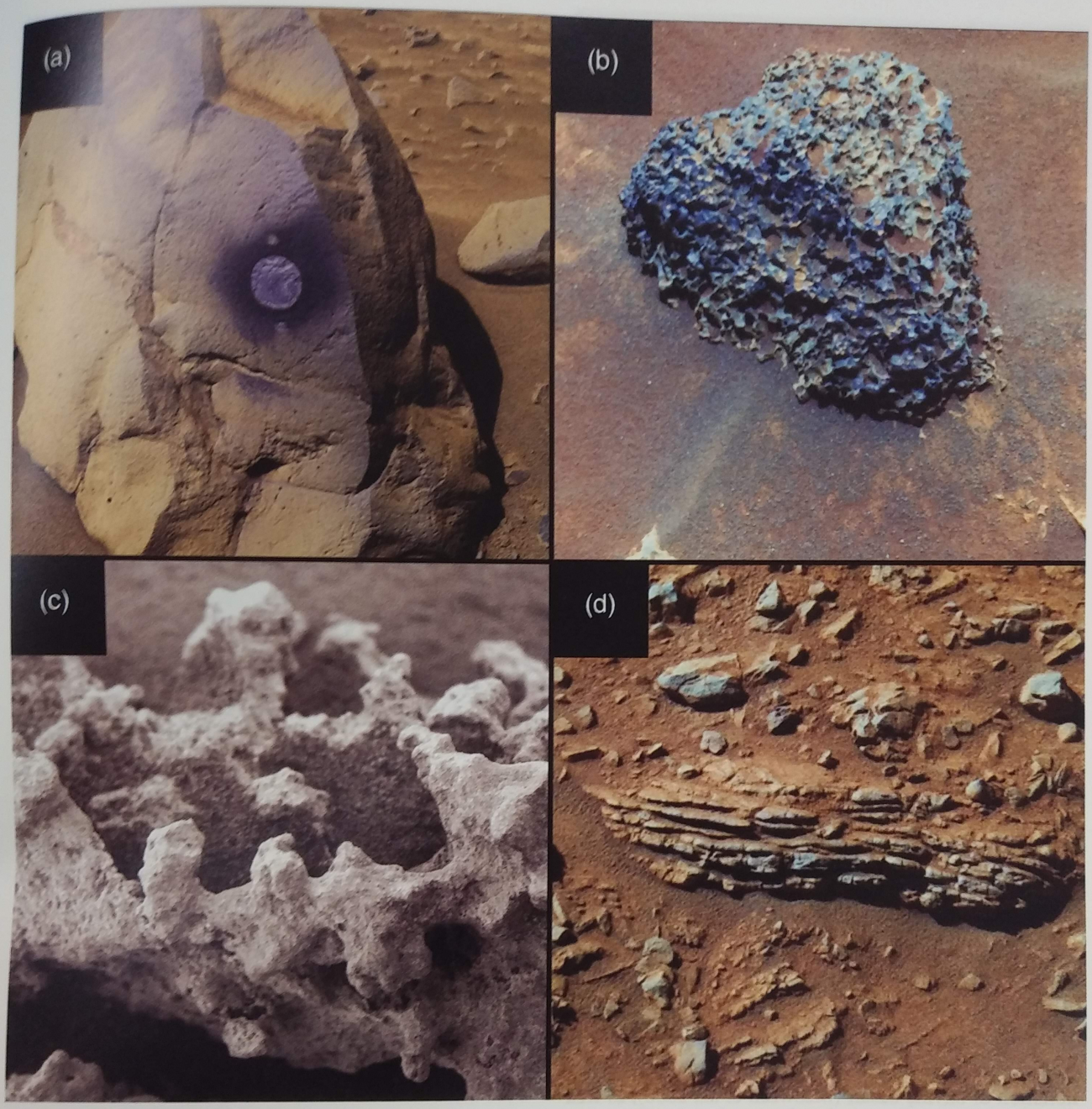

Figure 17.5 Rocks of Gusev crater, imaged by Spirit rover. (a) Plains basalt, with area ground by the rock abrasion tool, (b) scoria from the Inner Basin, (c) highly altered, friable rock from Columbia Hills, (d) layered rock from Columbia Hills. NASA images.

suggest multiple depositional and erosional events. Although previous studies (e.g., Grin and Cabrol, 1997) argued that lacustrine and fluvial processes formed the deposits on the floor of Gusev, Milam et al. (2003) could not rule out volcanic activity, and noted that the nearby Apollinaris volcano could have been the source of pyroclastic materials. Consequently, they favored a combination of volcanoclastic and sedimentary processes. Orbital spectroscopic data could not distinguish between these kinds of materials.

Spirit Rover's Surface Exploration

Spirit landed on ridged plains in Gusev, a surface consisting of abundant volcanic rocks (none of which are outcrops) resting on comminuted basaltic debris (Figure 17.5a). The rocks are fine-grained and porphyritic, sometimes with vesicles and vugs (Figure 17.5b). Compositions measured by APXS and mineralogy identified by spectroscopy indicate the rocks are olivine basalts (McSween et al., 2004), relatively unaltered but with surficial alteration rinds. Gusev contains no obvious

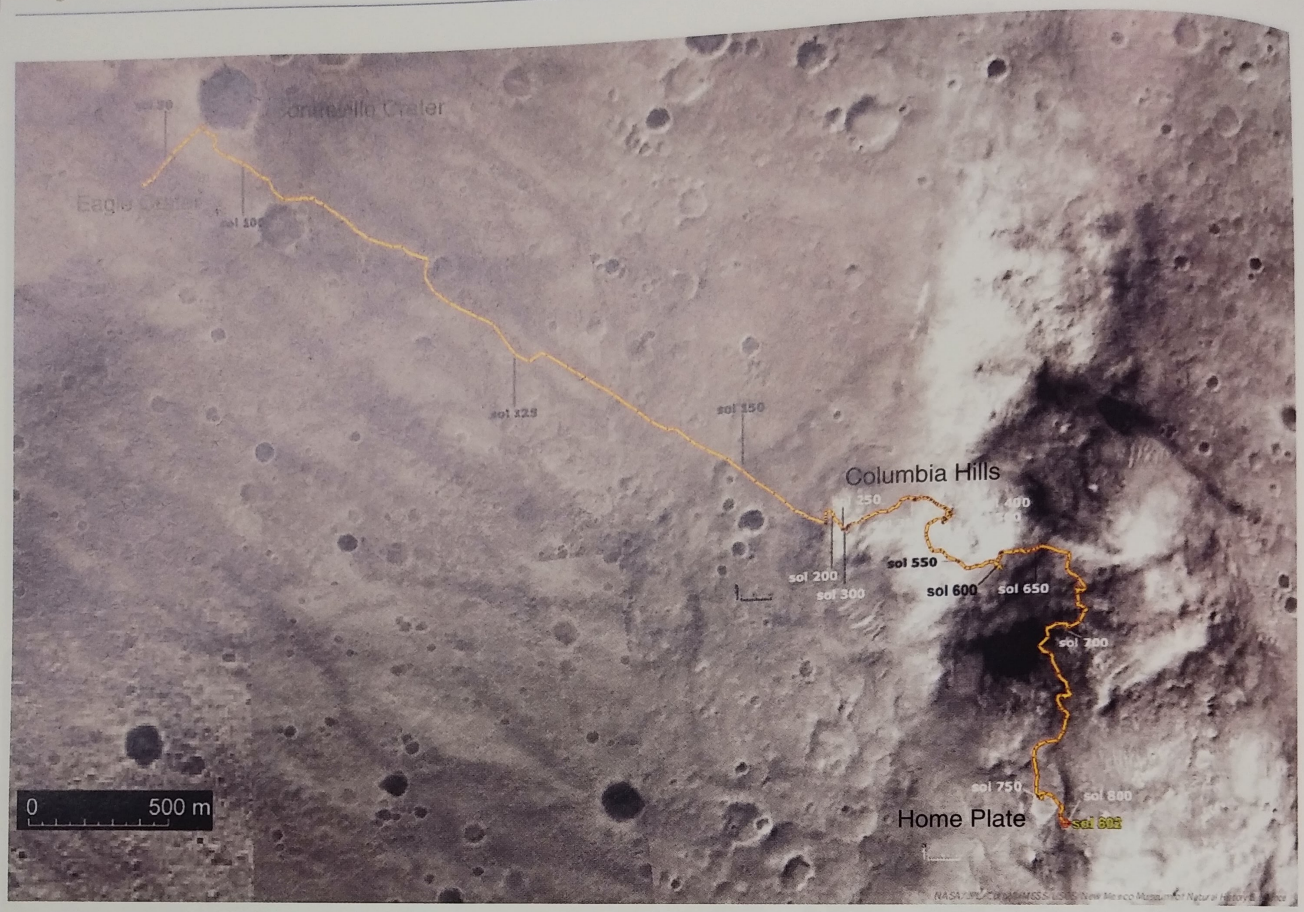

Figure 17.6 Traverse of the Spirit rover in Gusev crater.

eruption centers and flows from Apollinaris cannot be traced into the crater, so the basalts likely result from fissure eruptions within the crater.

After traversing to a nearby crater (Figure 17.6), Spirit trekked to the Columbia Hills, an older (Noachian?) uplifted unit that lies below the plains. Rocks in the Columbia Hills are highly varied in composition and texture (Figure 17.5c,d), and were extensively analyzed by Spirit's instruments. The rocks include lavas and pyroclastic rocks that could have been derived by fractionation of olivine basalt (McSween et al., 2006), as well as clastic sediments or impactites (Squyres et al., 2007).

Following exploration of the Columbia Hills, Spirit traversed through the Inner Basin to Home Plate (Figure 17.7), along the way encountering dark sand dunes and more basaltic rocks. Home Plate is a layered structure formed from pyroclastic materials of basaltic composition (Squyres et al., 2007). The rover wheels stirred up unusual soils rich in silica or sulfate, thought to have formed by hydrothermal processing. Spirit's mission ended when it became mired in soft sand near Home Plate.

The compositions of the alkaline volcanic rocks in Gusev crater were previously illustrated in Figure 10.14, and their petrogenesis was discussed in Section 10.4. None of the rocks encountered in Gusev are lacustrine sediments, as predicted before landing, indicating that any existing lake deposits must be buried by volcanic and impact materials.

17.3.2 Meridiani Planum

Orbital Studies

Based on orbital imagery, Meridiani Planum was originally interpreted as a layered sedimentary unit deposited in

Figure 17.7 Home Plate, consisting of layered pyroclastic rocks overlain by scoria. NASA image.

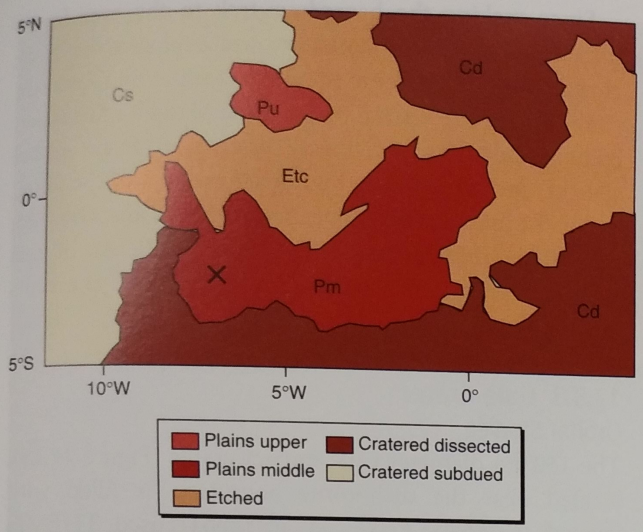

Figure 17.8 Geologic map of Meridiani Planum, simplified from Hynek et al. (2002). Opportunity's landing site is marked by X.

a closed basin (Edgett and Parker, 1997). A geologic map of the area (Figure 17.8) shows plains units that unconformably overlie etched units of the cratered highlands (Hynek et al., 2002). Arvidson et al. (2003) recognized that the Meridiani surface is dominated by basaltic sands and has been exhumed by erosion. The layered unit does not lie within any clearly defined basin, although a basin boundary has likely been destroyed by erosion. A proposed Late Noachian to Early Hesperian age of the layered unit was poorly defined. Because of erosion and infilling of smaller craters, the size–distribution curve does not follow a crater production curve.

Crystalline hematite covers a huge area (~150,000 km^2) coinciding with the middle plains unit in Meridiani Planum (Figure 17.9), as identified and mapped by orbital thermal emission spectra (Christensen et al., 2000). This widespread mineral is interpreted to have formed in an aqueous environment. Sulfates were also detected in Meridiani from orbital spectra (Gendrin et al., 2005).

Opportunity Rover's Surface Exploration

Opportunity came to rest in a small, shallow crater on a monotonously flat plain extending to the horizon in all directions. Examination and analysis of layered rocks in the crater wall showed them to be sandstones composed of basaltic detritus cemented by evaporates (mostly sulfates). Scattered throughout the rocks are hematite-bearing spherules (Figure 17.10a), referred to as "blueberries" (they are only blue in false-color images), which weather out and form a concentrated lag deposit on the pavement surface (Figure 17.10b) – this is the hematite detected from orbit. Hematite was identified using the Mössbauer spectrometer.

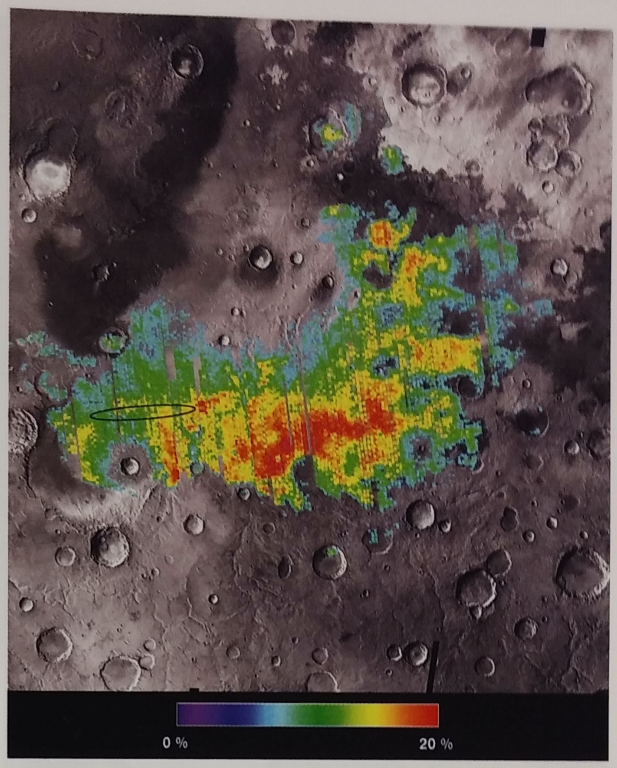

Figure 17.9 Distribution of hematite in Meridiani, The landing ellipse for the Opportunity rover is marked. NASA Mars Odyssey THEMIS map. Reproduced with permission from "Global mineralogy mapped from the Mars Global Surveyor Thermal Emission Spectrometer" by P. R. Christensen et al. within The Martian Surface edited by Jim Bell. © Cambridge University Press 2008.

Traversing to Endurance crater, Opportunity examined a vertical section of the hematite-sulfate unit, named the Burns formation (Figure 17.11). The interpreted stratigraphy is illustrated in the left column of Figure 17.12 (Grotzinger et al., 2005). A lower unit of cross-bedded sandstones formed as aeolian dunes. Finely laminated sandstones in the middle unit truncate cross-bedding of the lower unit. These sediments have been pervasively recrystallized and some dissolution of evaporate minerals has occurred, leaving casts (Figure 17.10a). The middle unit is interpreted as a sand sheet that marks a transition between the lower dune deposits and an upper unit of interdune deposits. The upper unit is characterized by coarse layering with festoon laminations – evidence of formation under subaqueous conditions.

The units of the Burns formation are interpreted to have formed by infiltration of groundwater to the surface to produce playa lakes in which basaltic mud was cemented by evaporates. Multiple groundwater recharge events formed the lower, middle, and upper units. A fourth infiltration produced the hematite concretions

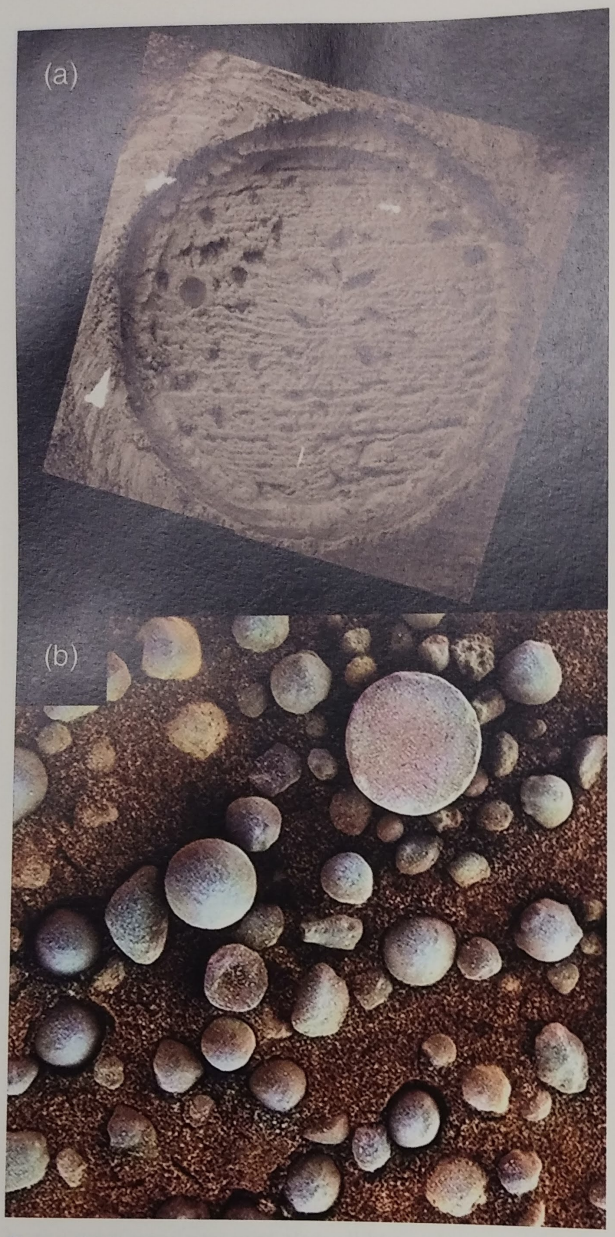

Figure 17.10 Hematite concretions at Meridiani, imaged by Opportunity rover. (a) RAT-ground rock showing layering, casts of dissolved minerals, and a blueberry, and (b) concentration of blueberries forming a lag deposit of hematite on the surface. NASA images.

that occur throughout the sequence (McLennan et al., 2005). The presence of the sulfate mineral jarosite indicates that the waters were highly acidic.

Following the analysis of strata in Endurance crater, Opportunity traversed to Victoria crater (Figure 17.13), an ancient impact scar with a rim scalloped by landslides. The rover circumnavigated a quarter of the way around the crater, investigating Burns formation layering in the walls (Figure 17.14).

Since making the hazardous trek to the even-larger Endeavour crater, Opportunity has explored the Noachian units that underlie the Burns formation (Arvidson et al., 2014). The layered rocks of the Matijevic formation contain smectites, previously discovered from orbital spectra, and are overlain by impact breccias of the Shoemaker formation and clastic sediments of the Grasberg formation (right column of Figure 17.12). As of this writing, Opportunity continues to explore the rim units of Endeavour.

17.3.3 Gale Crater

Orbital Studies

The 150 km diameter Gale impact crater (Figure 17.15), located near the dichotomy boundary, is filled with layered materials. Pelkey et al. (2004) used THEMIS images to map seven units in Gale crater, including crater walls, floor units, sand sheets, and a crescent-shaped central mound. Using visible and near-infrared images and topographic data, Le Deit et al. (2013) prepared the most current geologic map (Figure 17.16), and checked stratigraphic consistency using cross-sections.

The 5 km high central mound, now called Aeolis Mons (informally Mount Sharp), may contain the crater's central uplift at its core. The mound is covered with finely layered strata clearly visible from orbit. Based on geomorphology, almost every conceivable origin for the layered units in the mound has been proposed, including lava flows or ash-flow tuffs, sedimentary deposits of aeolian, fluvial or lacustrine origin, spring deposits, and ancient polar deposits (summarized by Le Deit et al., 2013). Orbital CRISM spectra show interstratified clay- and sulfate-bearing units (Figure 17.17) in the lower mound (bench) member (Thomson et al., 2011), ruling out a volcanic origin. Above an unconformity, the upper (caprock) member lacks signatures of either clays or sulfates (Milliken et al., 2010). Crater counting of the floor at the base of the mound gives an age of 3.6–3.8 Ga (Thomson et al., 2011; Le Deit et al., 2013), corresponding approximately to the Noachian–Hesperian boundary, and younger strata were deposited before ~3.2 Ga.

Curiosity Rover's Surface Exploration

Curiosity landed on a plain of shallowly dipping strata, now called the Bradbury group. The rover traversed these strata (Figure 17.18), eventually reaching the base of Aeolis Mons (Figure 17.19) and passing into the Mount Sharp group. The stratigraphy along the traverse of the Bradbury group is illustrated in Figure 17.20 (right column). During the early part of its traverse, Curiosity also encountered alkaline igneous rocks (Figure 17.21a,

Figure 17.11 Burns formation in Endurance crater. NASA image.

Stolper et al., 2013; Sautter et al., 2014), probably derived from the crater walls.

The Bradbury group consists of fluvial conglomerates (Figure 17.21b) and cross-bedded sandstones, as well as mudstones (Figure 17.21c). The rocks contain high proportions of igneous (basaltic) minerals, and the bulk chemistry of the rocks reflects their basaltic provenance (McLennan et al., 2014). Diagenesis is indicated by concretions and mineralized fractures (Figure 17.21d), and some of the sandstones are iron-cemented (Blaney et al., 2014). Clinoform sandstones in the sequence are interpreted as deltaic deposits formed where braided streams entered standing water (Grotzinger et al., 2015). The multiple clinoform layers at different elevations are thought to have been stacked during stream progradation.

The Murray formation, representing the basal unit of the Mount Sharp group, is a laminated mudstone overlain by cross-bedded or clinoform sandstone, interpreted as interfingering facies of deltaic sediments of the Bradbury group with finer-grained rocks of the Murray formation. Although its mineralogy is mostly basaltic minerals plus clays and amorphous material, an intermediate horizon contains silica (tridymite, cristobalite, quartz, and opal), suggesting a felsic source. In places, the base of the Murray formation is a conglomerate, and a hematite-bearing ridge overlies it. This formation represents a lacustrine facies adjacent to the fluvial–deltaic deposits (Grotzinger et al., 2015).

Above the Murray formation are clay-bearing strata that transition into polyhydrated sulfate-bearing strata (Figure 17.20, left column). Curiosity will continue to explore these units. Above the sulfate units is a caprock unit of unknown composition, with spectral signature similar to martian dust.

The reconstructed history of Gale (Grotzinger et al., 2015) posits that gravels eroded from the crater rim were transported inward by streams and deposited in a moat surrounding the crater's central uplift. These streams transitioned into sandy deltas marking the boundary of an ancient lake within which muds accumulated. Several kilometers of sediments were ultimately deposited. Following that, wind-driven erosion partly exhumed the strata by the Middle Hesperian Period, leaving Aeolis Mons as a surviving record of the sedimentary units that were removed.

17.4 Martian Meteorites: An Added Dimension

We do not know the exact provenance of any martian meteorites, although rayed craters may be likely launch sites (Tornabene et al., 2006). These craters are young, consistent with limited lifetimes of rays and with the short cosmic-ray exposure ages that are thought to date the times of ejection of the meteorites from Mars. The rayed craters are located in volcanic terrains, which accords with the meteorites' petrography. Hamilton et al. (2003) and Ody et al. (2015) identified terrains exhibiting thermal infrared and near-infrared spectra, respectively, that are similar to martian meteorites. The best shergottite analogs they found are Early Hesperian

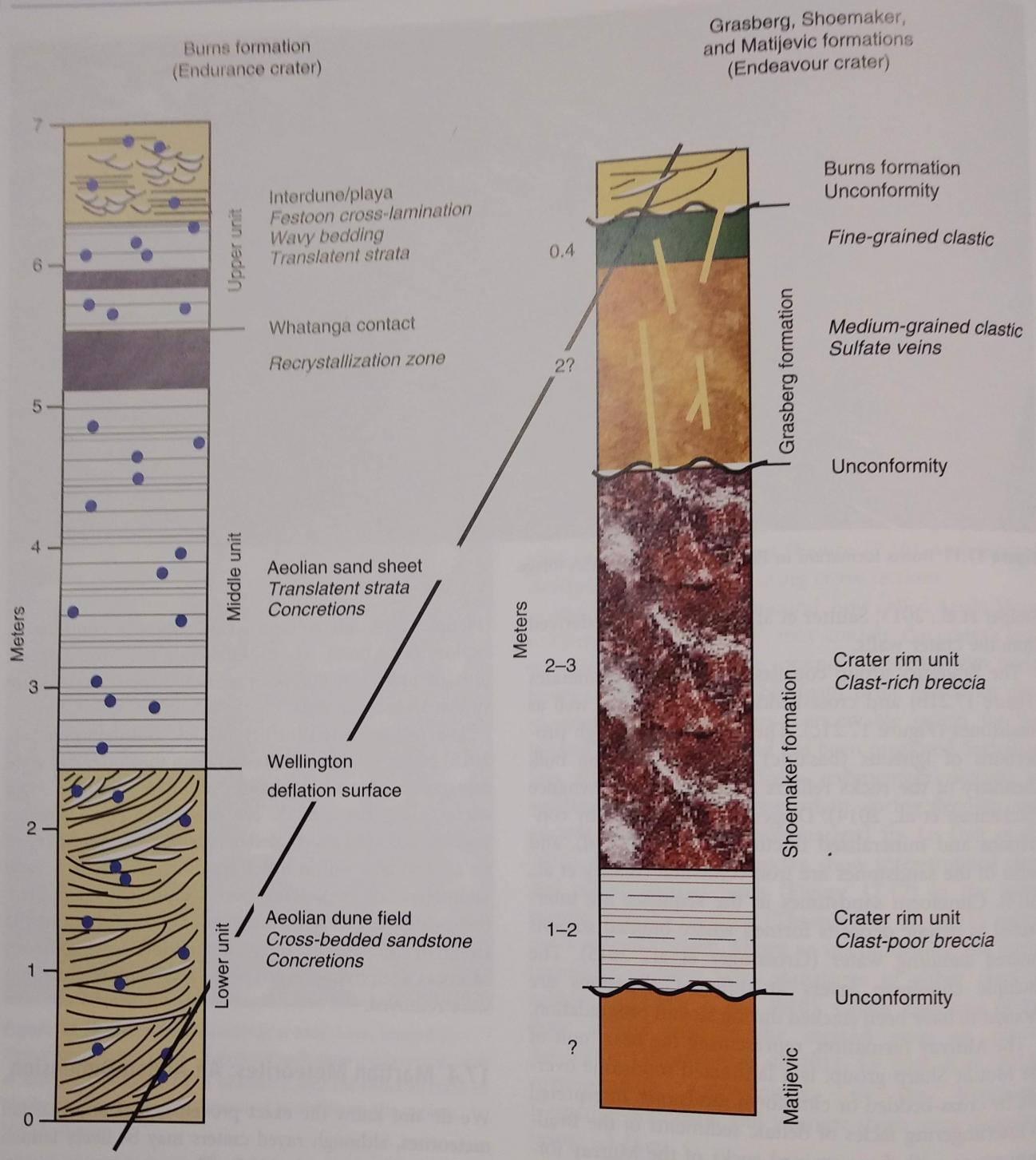

Figure 17.12 Meridiani stratigraphy, including the Burns formation mapped in Endurance crater (based on Grotzinger et al., 2005) and the underlying Noachian strata mapped in Endeavour crater (based on Grotzinger et al., 2015, and other data).

volcanic provinces (Syrtis Major, Hesperia Planum, Thaumasia Planum), but these regions are significantly older than shergottites; no nakhlite analogs were identified.

The petrology of the basaltic meteorites and related ultramafic cumulates was described in Section 10.4. Their predominantly young crystallization ages (<475 Ma for shergottites, 1.3 Ga for nakhlites/chassignites, 2.4 Ga for augite basalts) are Amazonian. Only one Noachian igneous cumulate rock, ALH 84001, is ~4.1 Ga. These ages indicate biased sampling, since most of the martian surface is Noachian. Identical cosmic-ray exposure ages for

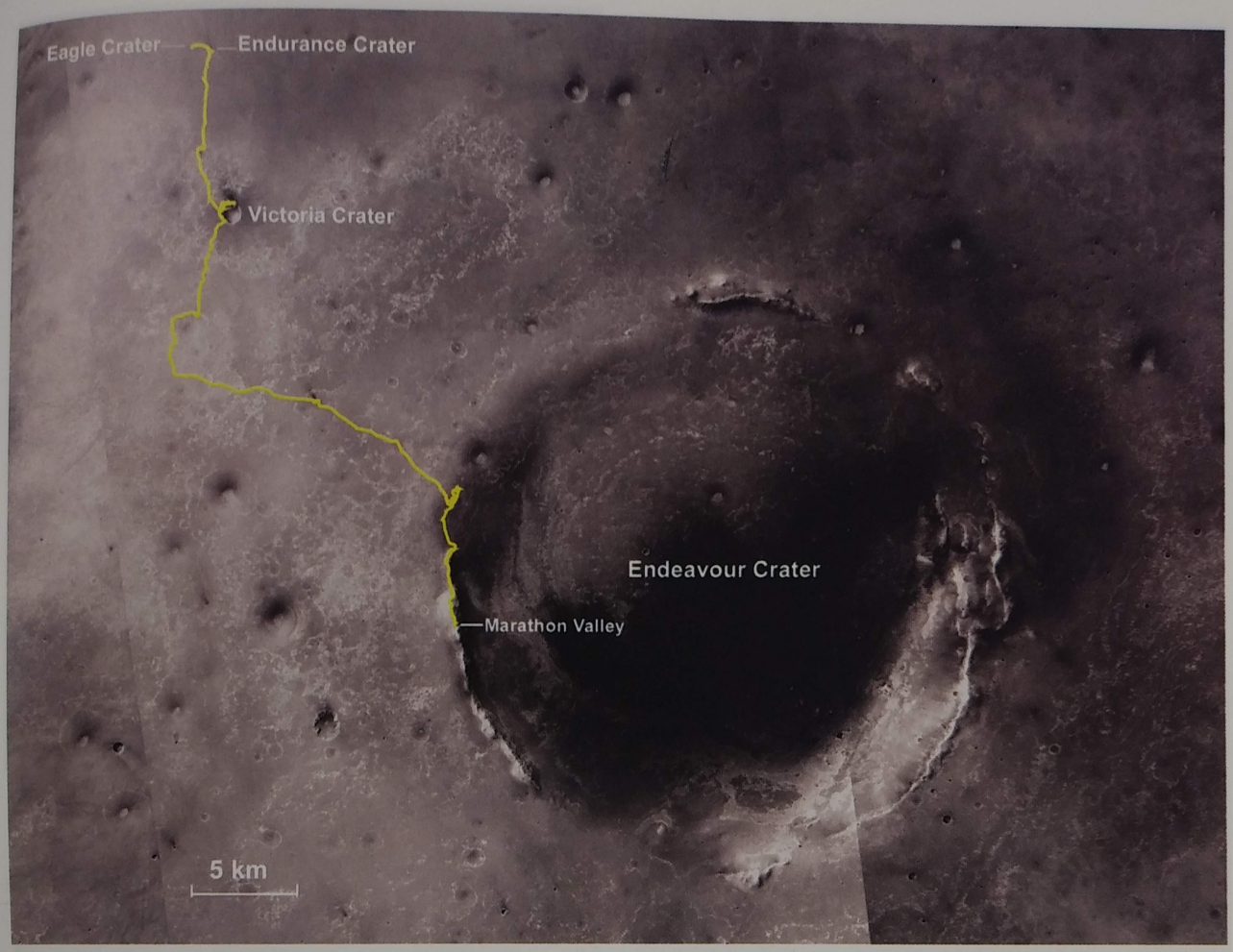

Figure 17.13 Traverse of the Opportunity rover in Meridiani Planum.

some shergottites and augite basalts suggest they sample the same location, and their widely varying crystallization ages imply a volcanic center (Tharsis?) that was intermittently active for billions of years (Lapen et al., 2017). Shergottites with different exposure ages indicate volcanism at a handful of other locations. The nakhlites represent a thick, fractionated flow similar in some respects to terrestrial komatiites, and demonstrate that basaltic shergottites were not the only Amazonian lavas.

Despite the young ages for most martian meteorites, they provide critical information on the origin and differentiation of Mars that is otherwise unobtainable. Radiogenic isotopes define the planet's time of accretion, and geochemical data indicate two distinct source regions that remained isolated for billions of years and were later melted or assimilated to produce the meteorites. It is unclear whether both the enriched and depleted sources reside in the mantle and were produced by solidification of a magma ocean (Debaille et al., 2007) or whether they represent enriched crust and depleted mantle, without the need for a magma ocean (Humayun et al., 2013). We also noted previously (Figure 10.14) that the meteorites are depleted in alkali elements relative to older rocks analyzed by Mars rovers in Gusev and Gale, implying magmatic evolution over time.

NWA 7034/7533 (Figure 15.6) and a few other paired meteorites are the only sedimentary martian meteorites. These Pre-Noachian regolith breccias are composed of clasts of alkaline igneous rocks (norites, pyroxenites, and monzonites) with crystallization ages of ~4.4 Ga, as well as various impact-melted materials. The ancient age indicates the existence of an igneous crust a little over 100 million years after the planet's accretion (Hewins et al., 2017). Geochemical characteristics of the clasts suggest that precursor rocks were hydrothermally altered, oxidized, and contained phyllosilicates. Abundant fine-grained magnetite and maghemite explain the meteorites' remanent paleomagnetism, and similar rocks may account for magnetism discovered in the ancient southern highlands.

Figure 17.14 Cross-bedded sandstones of the Burns formation in the wall of Victoria crater. NASA image.

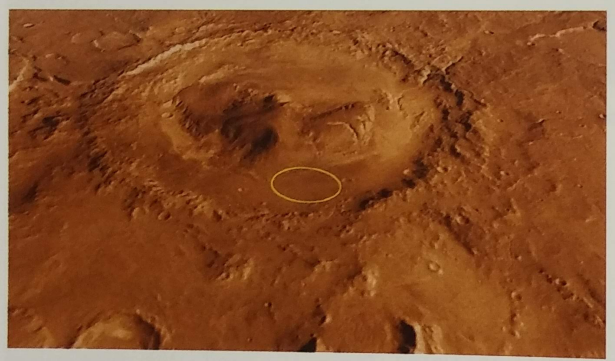

Figure 17.15 Image of Gale crater, showing the central mound. The yellow oval represents the landing ellipse for the Curiosity rover prior to arrival. NASA image.

17.5 Integration and Synthesis

The results of decades of exploration by orbiters, landers, and rovers, and of the analyses of martian meteorites, have been integrated to form an understanding of the geologic history of Mars. The summary below is adapted from comprehensive reviews of martian geology (Carr, 2006; Carr and Head, 2010; Tanaka et al., 2014), geochemistry (McSween and McLennan, 2014), and mineralogy/petrology (Bell, 2008; McSween, 2015). It is not

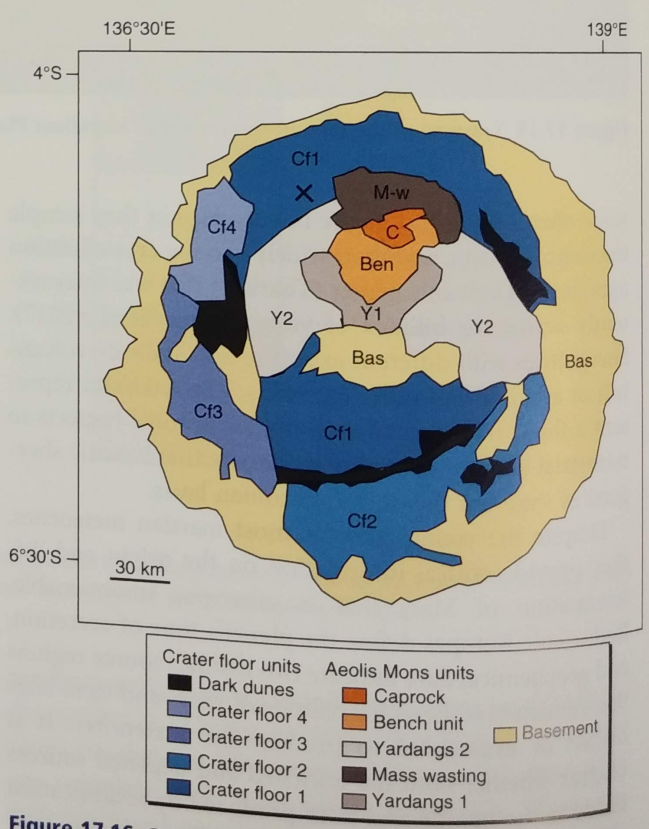

Figure 17.16 Geologic map of Gale crater, simplified from Le Deit et al. (2013). Curiosity's landing site is marked by X.

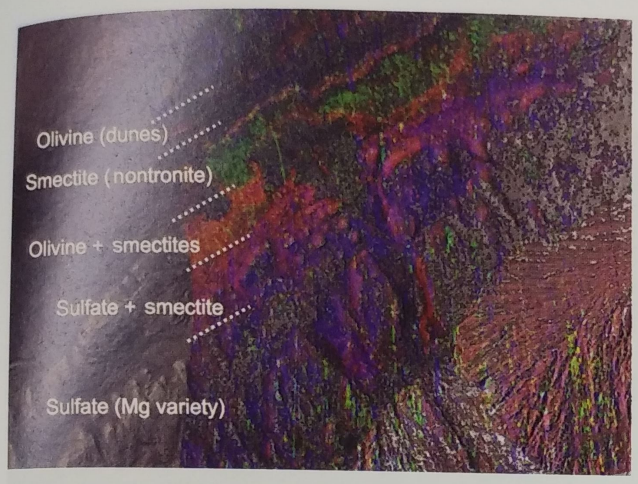

Figure 17.17 Mineralogy on the slope of Aeolis Mons, as mapped by CRISM spectra from the *Mars Reconnaissance Orbiter*. Modified from Milliken et al. (2014).

possible to cite the hundreds of papers that have added meaningfully to this effort, so we won't even try, but those references can be found in the above reviews.

Figure 17.22 presents a simplified view of the geologic evolution of Mars, with each period described below. The crystallization ages of martian meteorites are shown on the right side, and the Earth's geologic eras are compared on the left.

17.5.1 Pre-Noachian Period

No units recognizable at the scale of orbital spacecraft mapping survive from Pre-Noachian time, so little is directly known. Mars accreted and rapidly differentiated into crust, mantle, and core within the first few tens of millions of years of Solar System history, as indicated by the decay products of extinct radionuclides in martian meteorites. It is possible that the planet had an early

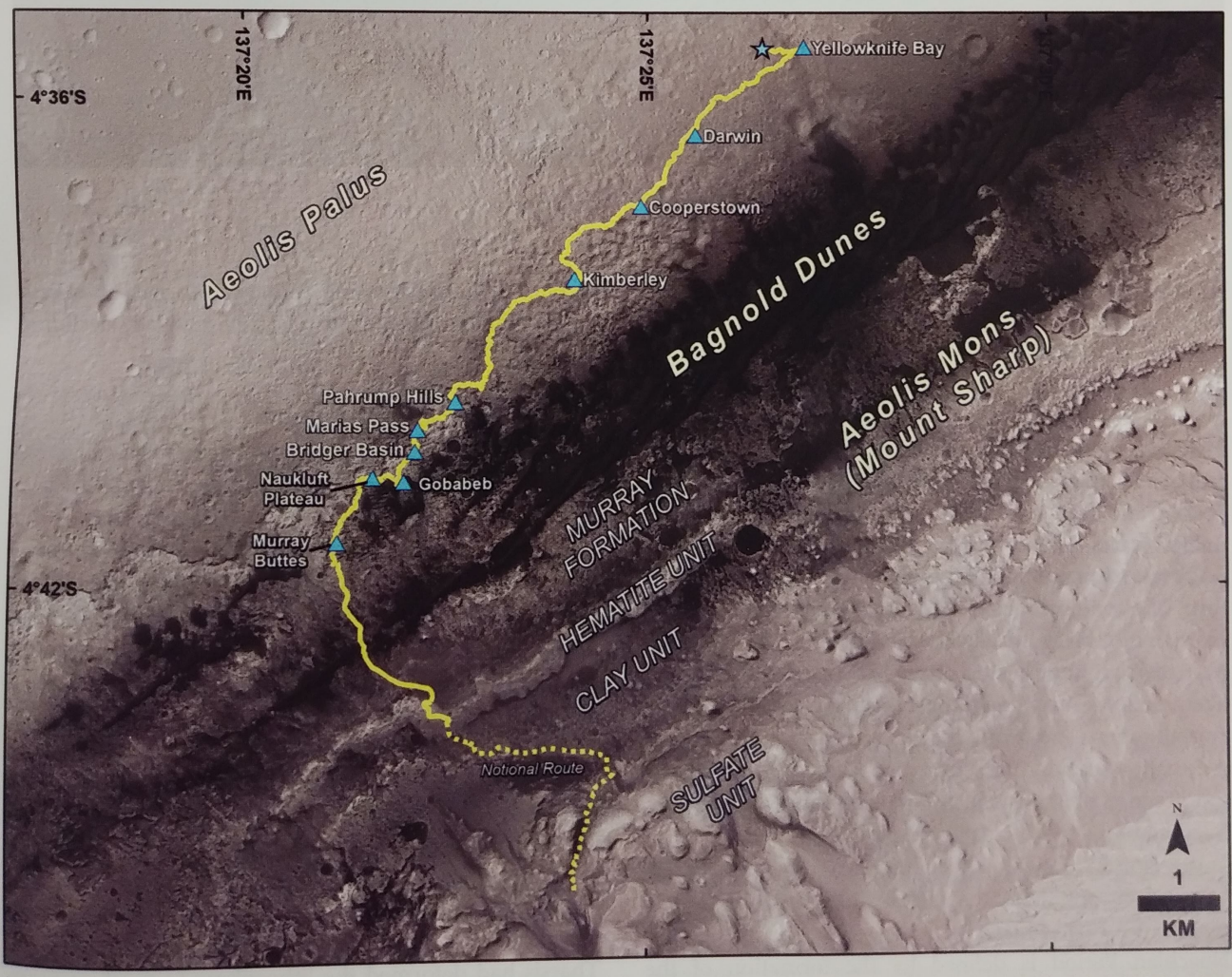

Figure 17.18 Traverse of the Curiosity rover in Gale crater.

Figure 17.19 Approach image of Aeolis Mons, taken by NASA Curiosity rover.

magma ocean that facilitated core segregation and that fractionally crystallized to form the distinct mantle source regions recognized in later-formed basaltic meteorites. The martian core consists of FeNi metal and FeS. An early dynamo resulted in striped magnetic anomalies in the highlands, possibly produced by iron minerals in the deep crust, and then declined by the Noachian. Heat flow peaked and then declined during the first few hundred million years. The ancient crust may have formed by decompression melting of mantle during convective overturn. The compositions of clasts in the only Pre-Noachian martian meteorites are alkaline basaltic rocks. The absence of a martian anorthositic crust, like that on the Moon, likely follows from water that suppressed plagioclase crystallization and from higher pressures that allowed segregation of aluminum into garnet at depth. Similarly, the absence of granitic crust reflects limited magmatic fractionation and no crustal recycling by subduction.

Pre-Noachian time was subject to numerous basin-forming impacts, and the global dichotomy itself may represent a huge impact structure. The end of the Pre-Noachian Period is defined by the formation of the 2400 km diameter Hellas basin variously assigned as ~4.1–3.8 Ga (depending on whether it formed in a Late Heavy Bombardment or in a time of gradually declining impacts).

17.5.2 Noachian Period/System

The Noachian Period was also distinguished by high but rapidly declining rates of cratering. In their global geologic map, Tanaka et al. (2014) distinguished units formed during the Early, Middle, and Late Noachian Epochs in the highlands, respectively containing 65, 15, and 2 impact basins >150 km in size. These impacts would have distributed ejecta over the globe, brecciated the upper crust, and promoted hydrothermal metamorphism beneath and around craters.

Magmatism during this period was likely concentrated in Tharsis, resulting in accumulation of a volcanic pile 9 km high and 5000 km across, equivalent to a global layer of lavas 2 km thick. If the magmas contained amounts of volatiles similar to Hawaiian basalts, they could have outgassed water equivalent to a global layer 120 m deep. By the end of the Noachian, the formation of Tharsis had deformed the lithosphere to produce a surrounding trough and a pronounced gravity anomaly, as

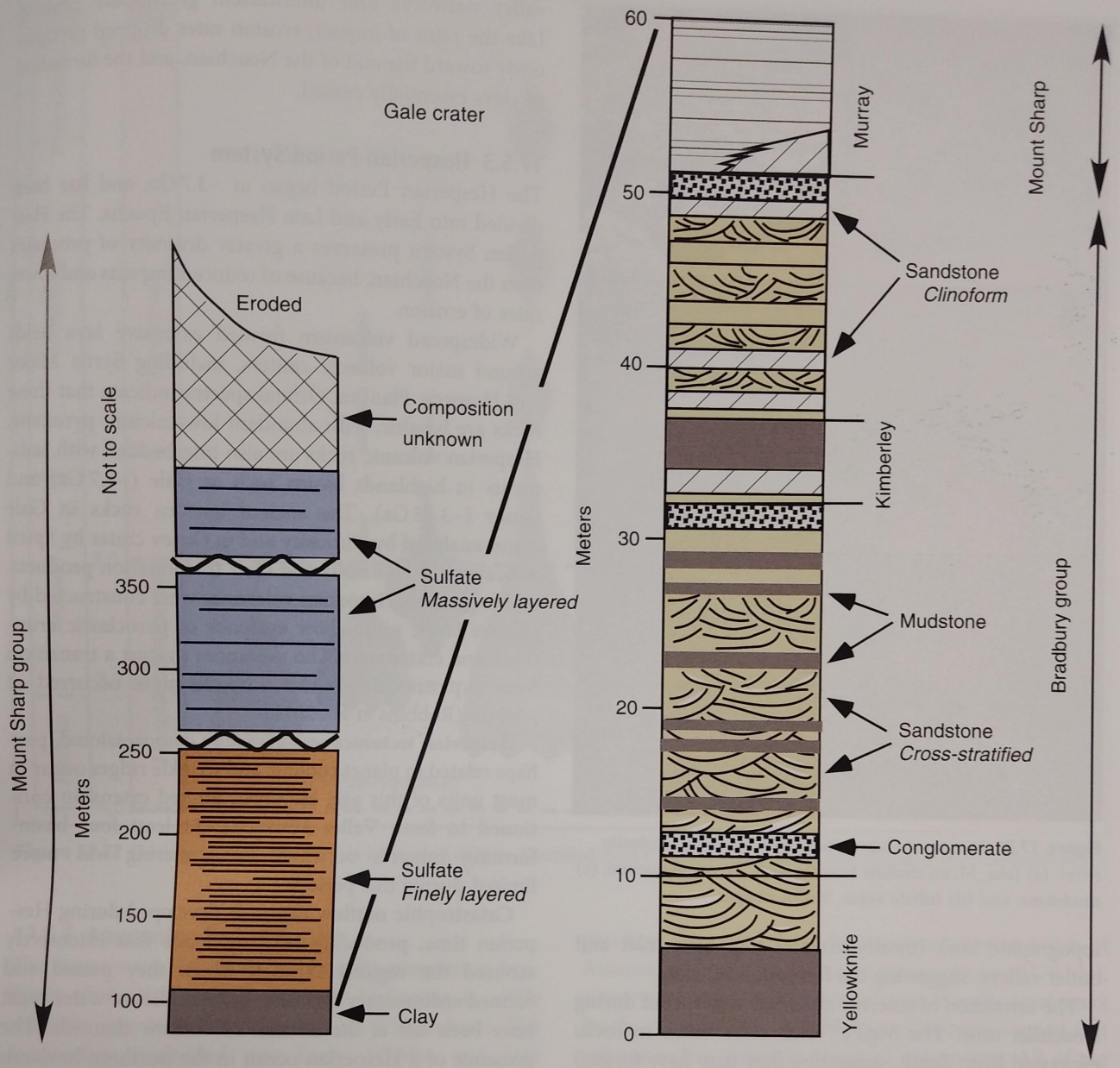

Figure 17.20 Stratigraphy of Gale crater. The right column shows the already-explored Bradbury group and lower portion of the Mount Sharp group in Gale crater, modified from Grotzinger et al. (2015). The left column (note change in vertical scale) shows the as-yet unexplored stratigraphy of Aeolis Mons, modified from Milliken et al. (2014).

predicted by loading of a spherical elastic shell. Extensional tectonics produced grabens, including rifting that initiated the formation of Valles Marineris. Most of the rocks in the southern highlands are probably Noachian basalts and pyroclastics reworked by impacts and sedimentation. Orbital spectra indicate the basalts are dominated by low-calcium pyroxene and sometimes olivine. The NWA 7034/7533 meteorite breccia (4.4 Ga) contains clasts of alkaline mafic igneous rocks, and the ALH 84001 martian meteorite (4.1 Ga) is an ultramafic cumulate from a basaltic magma, but the Noachian is otherwise so far unsampled as meteorites, likely because of the difficulty of ejecting brecciated rocks.

Noachian surface conditions enabled rapid erosion and surface degradation that produced large amounts of debris. Craters of this age generally have highly eroded rims and are filled with sediments. Estimated erosion rates were 2–5 orders of magnitude higher than in subsequent periods, but even so, they were lower than erosion rates on Earth. Noachian terrains are dissected by valley networks, which have been attributed to both groundwater sapping and precipitation. The networks drain into

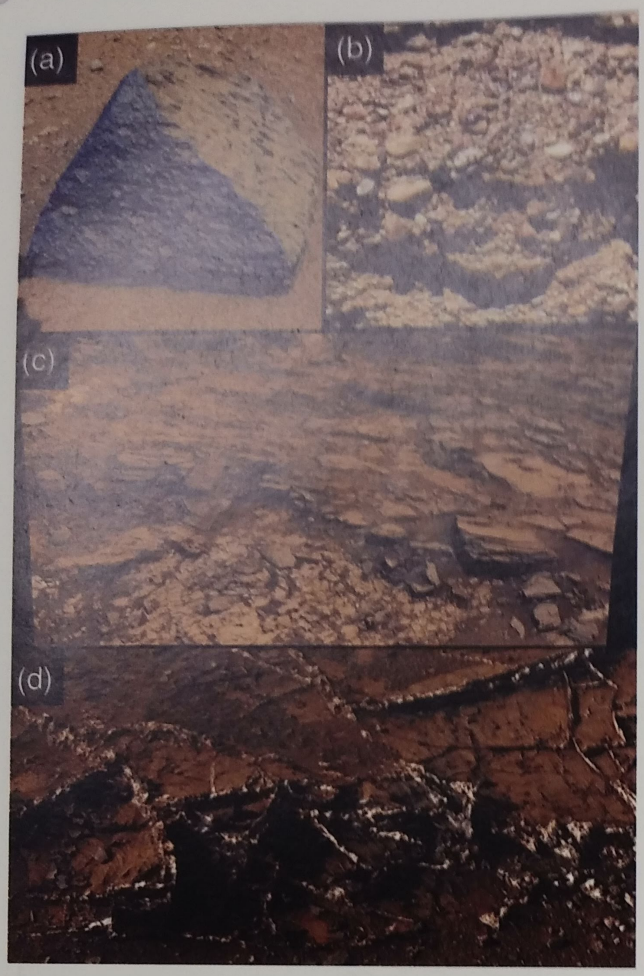

Figure 17.21 Images of Gale crater rocks, taken by Curiosity rover. (a) Jake_M, an alkaline basaltic rock, (b) conglomerate, (c) mudstone, and (d) sulfate veins. NASA images.

topographic lows (mostly craters) that have inlet and outlet valleys, suggesting the formation of lakes.

The formation of smectite clays was widespread during Noachian time. The Mg,Fe^{2+}-rich clays occur in rocks excavated from depth, suggesting they may have formed by diagenesis or hydrothermal metamorphism of mafic rocks, whereas Al,Fe^{3+}-rich clays likely formed by surficial chemical weathering (Ehlmann et al., 2011; Bishop et al., 2018). Serpentine and talc also occur. Although much speculation about Noachian climate is based on the assumption of weathering, the evidence for groundwater and lakes is most consistent with only episodically warm conditions. Even with an atmosphere enhanced with greenhouse gases from volcanic outgassing, climate models cannot produce the global average temperatures that would sustain liquid water at the surface. The lack of significant carbonate deposits does not support ideas of a dense CO_2 atmosphere that would support greenhouse warming. Perhaps large impacts or volcanic eruptions released H_2O that could account for precipitation to form valley networks and intermittent greenhouse heating. Like the rates of impact, erosion rates dropped precipitously toward the end of the Noachian, and the formation of clays essentially ceased.

17.5.3 Hesperian Period/System

The Hesperian Period began at ~3.7 Ga, and has been divided into Early and Late Hesperian Epochs. The Hesperian System preserves a greater diversity of processes than the Noachian, because of reduced impacts and lower rates of erosion.

Widespread volcanism formed extensive lava fields around major volcanic centers, including Syrtis Major and Hesperia Planum. Orbital spectra indicate that these rocks are basaltic, with abundant low-calcium pyroxene. Hesperian volcanic rocks are also interbedded with sediments in highlands basins such as Gale (~3.7 Ga) and Gusev (~3.65 Ga). The ancient igneous rocks in Gale crater analyzed by Curiosity and in Gusev crater by Spirit indicate alkaline basalts and their fractionation products. Although most Hesperian volcanoes were constructed by effusive lavas, some show evidence of pyroclastic eruptions, and crater counts on volcanoes suggest a transition from explosive to effusive eruption style occurred at ~3.5 Ga (Robbins et al., 2011).

Hesperian tectonics was generally compressional, perhaps related to planet cooling, and wrinkle ridges occur in most units of this age. However, limited extension continued to form Valles Marineris. At least four basin-forming impacts occurred, but cratering was more limited during this period.

Catastrophic outflow channels developed during Hesperian time, producing massive floods that extensively scoured the regions through which they passed and formed sedimentary deposits. Large bodies of water must have been left at the termini of outflow channels. The presence of a Hesperian ocean in the northern lowlands has also been advocated, although compelling evidence is as yet lacking. The formation of valley networks declined significantly during the Hesperian, indicating a progressive change in environmental conditions. Sulfate- and chloride-rich deposits, as found in Meridiani and Gale, suggest evaporation of lakes, possibly due to oscillations in the groundwater table. The orbital detection of widespread olivine in Hesperian units indicates that weathering was very limited.

The oldest ice-bearing units in the martian polar deposits are of Hesperian age. These may have formed by cryovolcanic eruptions or from accumulation of a glacial ice sheet. The end of the Hesperian is defined as the cessation of deposition of sedimentary plains in the northern lowlands.

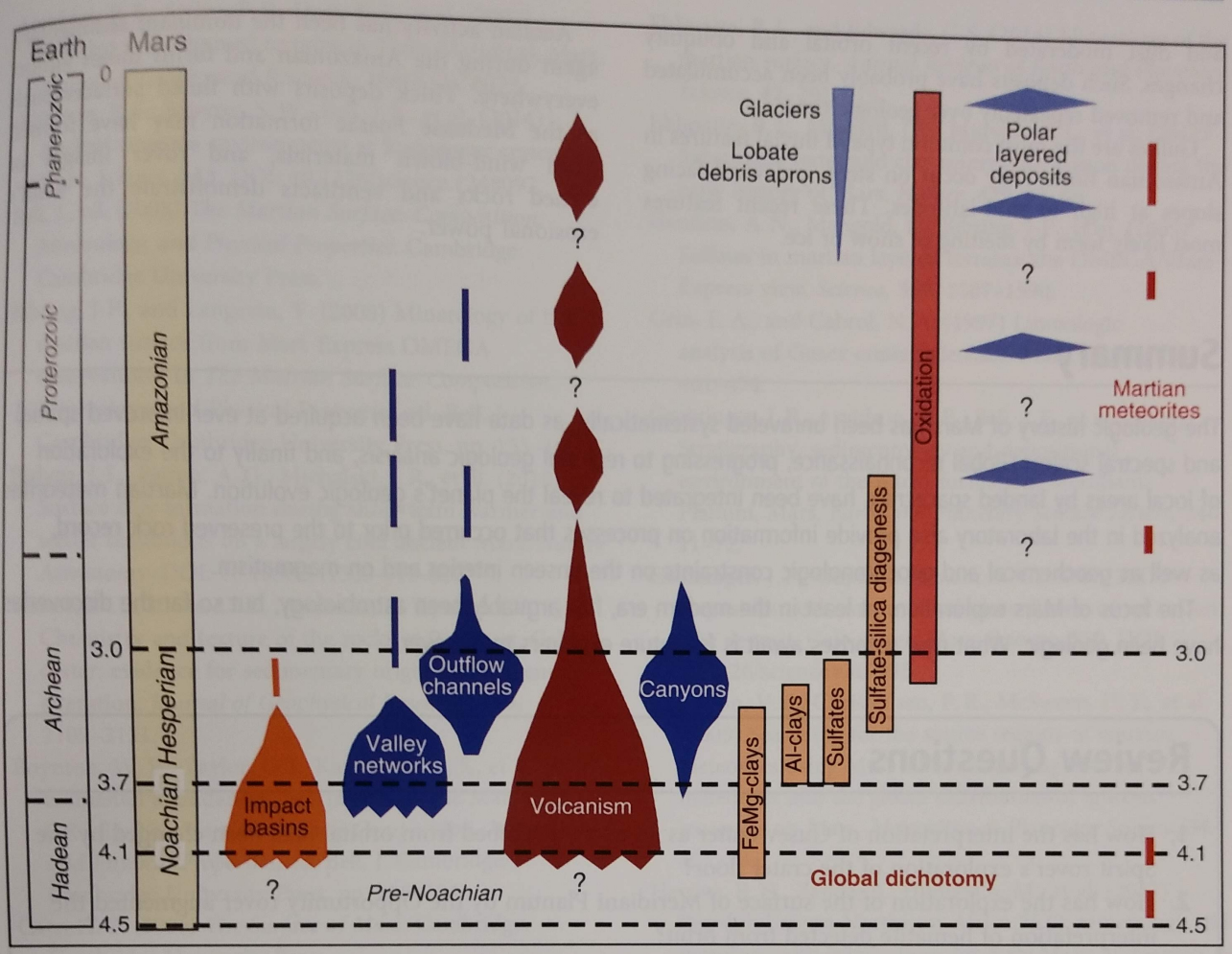

Figure 17.22 Geologic activity on Mars, as a function of time. Modified from Carr and Head (2010) and Ehlmann and Edwards (2014).

17.5.4 Amazonian Period/System

The Amazonian Period is the longest, comprising two-thirds of martian geologic time. Its beginning at ~3 Ga coincides approximately with the Earth's Archean. The Amazonian is divided into Early, Middle, and Late Epochs. Despite the period's long duration, the geomorphic effects of cratering, volcanism, and tectonism are modest. The effects of ice and wind are more prominent in Amazonian units, owing to the low rates of erosion and landscape construction by other processes. The environment has been cold, dry, and oxidizing, leading to widespread formation of hematite that gives Mars its red color.

Amazonian volcanism was mostly confined to Tharsis and Elysium, where large shields continued to grow episodically. Lava flows are prominent and suggest more limited outpourings relative to the flood basalt style of the Hesperian volcanic plains. In contrast to Noachian and Hesperian basalts dominated by low-calcium pyroxene, the Amazonian basalts contain mostly high-calcium pyroxene. The ages of martian meteorites span much of Amazonian time. The youngest shergottite ages (175 Ma), along with crater-density ages of tens of millions of years for the youngest flows in Tharsis and Elysium, suggest that volcanism has persisted nearly to the present. All of the basaltic meteorites and associated cumulates formed from tholeiitic rather than alkaline magmas. Most Amazonian flows are not deformed by wrinkle ridges, but some limited development of narrow grabens and wrinkle ridges may have resulted from local crustal loading by lavas.

The effects of ice include ice-dust veneers covering the planet's surface at mid- to high latitudes, ground ice, possible glacial effects on some volcanoes, ice-cored debris aprons at mid-latitudes, and polar deposits. The presence of present-day near-surface ice has been detected by orbital gamma ray/neutron measurements of hydrogen, and the *Phoenix* lander confirmed the occurrence of a shallow ice table. Ice stability is sensitive to the obliquity cycle, which varies considerably on Mars. Thinly layered polar deposits are accumulations of ice

and dust moderated by recent orbital and obliquity changes. Such deposits have probably been accumulated and removed repeatedly over geologic time.

Gullies are the most common type of fluvial features in Amazonian time. They occur on steep, poleward-facing slopes at high to mid-latitudes. These recent features most likely form by melting of snow or ice.

Aeolian activity has been the dominant sedimentary agent during the Amazonian and forms dunes almost everywhere. Thick deposits with fluted surfaces such as the Medusae Fossae formation may have formed from wind-blown materials, and rover images of etched rocks and ventifacts demonstrate the wind's erosional power.

Summary

The geologic history of Mars has been unraveled systematically, as data have been acquired at ever-improved spatial and spectral scales. Global reconnaissance, progressing to regional geologic analysis, and finally to the exploration of local areas by landed spacecraft, have been integrated to reveal the planet's geologic evolution. Martian meteorites analyzed in the laboratory also provide information on processes that occurred prior to the preserved rock record, as well as geochemical and geochronologic constraints on the unseen interior and on magmatism.

The focus of Mars exploration, at least in the modern era, has arguably been astrobiology, but so far the discoveries have been geologic. What new surprises await is for future explorers to discover.

Review Questions

1. How has the interpretation of Gusev crater as an ancient lakebed from orbital data been changed by the Spirit rover's exploration of the crater floor?
2. How has the exploration of the surface of Meridiani Planum by the Opportunity rover augmented the interpretation of hematite detected from orbit?
3. How has the Curiosity rover's exploration complemented orbital remote sensing of Gale crater?
4. Give two examples of how the analysis of martian meteorites has improved our understanding of the unseen interior of Mars.
5. What are the first-order changes in geologic processes that characterized the Noachian, Hesperian, and Amazonian Periods?

SUGGESTIONS FOR FURTHER READING

Bell, J., ed. (2008) *The Martian Surface: Composition, Mineralogy, and Physical Properties*. Cambridge: Cambridge University Press. These 27 chapters are a goldmine of information about the geologic exploration of the surface of Mars.

Carr, H. Y. (2006) *The Surface of Mars*. Cambridge: Cambridge University Press. An authoritative book on the geology of Mars.

Carr, M. H., and Head, J. W. (2010) Geologic history of Mars. *Earth and Planetary Science Letters*, **294**, 185–203. A clear and concise summary of the geologic evolution of Mars.

McSween, H. Y., and McLennan, S. M. (2014) Mars. In *Treatise in Geochemistry*, Vol. 2, 2nd edition, eds. Holland, H. D., and Turekian, K. K. Oxford: Elsevier, pp. 251–300. The geochemistry of Mars, from A to Z.

Tanaka, K. L., Skinner, J. A., Dohm, J. M., et al. (2014) Geologic map of Mars. US Geological Survey Scientific Investigations Map 3292. The most recent iteration of a global geologic map for Mars. An accompanying pamphlet provides details on how the map was crafted.

REFERENCES

Acuna, M. H., Kletetschka, G., and Connerney, J. E. P. (2008) Mars' crustal magnetism: a window into the past. In *The Martian Surface: Composition, Mineralogy, and Physical Properties*, ed. Bell, J. Cambridge: Cambridge University Press, pp. 242–262.

Arvidson, R. E., Seelos, F. P., Deal, K. S., et al. (2003) Mantled and exhumed terrains in Terra Meridiani, Mars. *Journal of Geophysical Research*, **108**(E12), 8073.

Arvidson, R. E., Squyres, S. W., Bell, J. F., et al. (2014) Ancient aqueous environments at Endeavour crater, Mars. *Science*, **343**. DOI: 10.1126/science.1248097.

Bell, J., ed. (2008) *The Martian Surface: Composition, Mineralogy, and Physical Properties*. Cambridge: Cambridge University Press.

Bibring, J-P., and Langevin, Y. (2008) Mineralogy of the martian surface from Mars Express OMEGA observations. In *The Martian Surface: Composition, Mineralogy, and Physical Properties*, ed. Bell, J. Cambridge: Cambridge University Press, pp. 153–168.

Bishop, J. L., Fairen, A. G., Michalski, J. R., et al. (2018) Surface clay formation during short-term warmer and wetter conditions on a largely cold ancient Mars. *Nature Astronomy*. DOI: 10.1038/s41550-017-0377-9.

Blaney, D. L., Blake, D. F., Vaniman, D. T., et al. (2014) Chemistry and texture of the rocks at Rocknest, Gale crater: evidence for sedimentary origin and diagenetic alteration. *Journal of Geophysical Research*, **119**, 2109–2131.

Boynton, W. V., Taylor, G. J., Karunatillake, S., et al. (2008) Elemental abundances determined via the Mars Odyssey GRS. In *The Martian Surface: Composition, Mineralogy, and Physical Properties*, ed. Bell, J. Cambridge: Cambridge University Press, pp. 105–124.

Carr, H. Y. (2006) *The Surface of Mars*. Cambridge: Cambridge University Press.

Carr, M. H., and Head, J. W. (2010) Geologic history of Mars. *Earth and Planetary Science Letters*, **294**, 185–203.

Christensen, P. R., Clark, R. N., Kieffer, H. H., et al. (2000) Detection of crystalline hematite mineralization on Mars by the Thermal Emission Spectrometer: evidence for near-surface water. *Journal of Geophysical Research*, **105**, 9623–9642.

Christensen, P. R., Bandfield, J. L., Fergason, R. L., et al. (2008) The compositional diversity and physical properties mapped from the Mars Odyssey Thermal Emission Imaging System. In *The Martian Surface: Composition, Mineralogy, and Physical Properties*, ed. Bell, J. Cambridge: Cambridge University Press, pp. 221–241.

Debaille, V., Brandon, A. D., Yin, Q. Z., et al. (2007) Coupled ^{142}Nd-^{143}Nd evidence for a protracted magma ocean on Mars. *Nature*, **450**, 525–528.

Edgett, K. S., and Parker, T. J. (1997) Water on early Mars: possible subaqueous sedimentary deposits covering ancient crater terrain in western Arabia and Sinus Meridiani. *Geophysical Research Letters*, **24**, 2897–2900.

Ehlmann, B. L., and Edwards, C. S. (2014) Mineralogy of the martian surface. *Annual Reviews of Earth and Planetary Science*, **42**, 291–315.

Ehlmann, B. L., Mustard, J. F., Murchie, S. L., et al. (2011) Subsurface water and clay mineral formation during the early history of Mars. *Nature*, **479**, 53–60

Gendrin, A. N., Mangold, N., Bibring, J-P., et al. (2005) Sulfates in martian layered terrains: the OMEGA/Mars Express view. *Science*, **307**, 1587–1590.

Grin, E. A., and Cabrol, N. A. (1997) Limnologic analysis of Gusev crater paleolake, Mars. *Icarus*, **130**, 461–474.

Grotzinger, J. P., Arvidson, R. E., Bell, J. F., et al. (2005) Stratigraphy, sedimentology and depositional environment of the Burns formation, Meridiani Planum, Mars. *Earth and Planetary Science Letters*, **240**, 11–72.

Grotzinger, J. P., Gupta, S., Malin, M. C., et al. (2015) Deposition, exhumation, and plaeoclimate of an ancient lake deposit, Gale crater, Mars. *Science*, **350**. DOI: 10.1126/science.aac7575.

Hamilton, V. E., Christensen, P. R., McSween, H. Y., et al. (2003) Searching for the source regions of martian meteorites using MGS TES: integrating martian meteorites into the global distribution of igneous materials on Mars. *Meteoritics & Planetary Science*, **38**, 871–885.

Hewins, R. H., Zanda, B., Humayun, M., et al. (2017) Regolith breccia Northwest Africa 7533: mineralogy and petrology with implications for early Mars. *Meteoritics & Planetary Science*, **52**, 89–124.

Humayun, M., Nemchin, A., Zanda, B., et al. (2013) Origin and age of the earliest martian crust from meteorite NWA 7533. *Nature*, **503**, 513–517.

Hynek, B. M., Arvidson, R. E., and Phillips, R. J. (2002) Geologic setting and origin of Terra Meridiani hematite deposits on Mars. *Journal of Geophysical Research*, **107**(E10), 5088.

Kuzmin, R. O., Greeley, R., Landheim, R., et al. (2000) Geologic map of the MTM-15182 and MTM-15187 quadrangles, Gusev crater–Ma'adim Vallis region, Mars. USGS Geologic Investigations Series.

Lapen, T. J., Righter, M., Andreasen, R., et al. (2017) Two billion years of magmatism recorded from a single Mars meteorite ejection site. *Science Advances*, **3**. DOI: 10.1126/scieadv.1600922.

Le Deit, L., Hauber, E., Fueten, F., et al. (2013) Sequence of infilling events in Gale crater, Mars: results from morphology, stratigraphy, and mineralogy. *Journal of Geophysical Research*, **118**, 2439–2473.

McLennan, S. M., Bell, J. F., Calvin, W. M., et al. (2005) Evidence for groundwater involvement in the

provenance and diagenesis of the evaporaite-bearing Burns formation. *Earth and Planetary Science Letters*, **240**, 95–121.

McLennan, S. M., Anderson, R. B., Bell, J. F., et al. (2014) Elemental geochemistry of sedimentary rocks at Yellowknife Bay, Gale crater, Mars. *Science*, **343**. DOI: 10.1126/science.1243480.

McSween, H. Y. (2015) Petrology on Mars. *American Mineralogist*, **100**, 2380–2395.

McSween, H. Y., and McLennan, S. M. (2014) Mars. In *Treatise in Geochemistry*, Vol. 2, 2nd edition, eds. Holland, H. D., and Turekian, K. K. Oxford: Elsevier, pp. 251–300.

McSween, H. Y., Arvidson, R. E., Bell, J. F., et al. (2004) Basaltic rocks analyzed by the Spirit rover in Gusev crater. *Science*, **305**, 842–845.

McSween, H. Y., Ruff, S. W., Morris, R. V., et al. (2006) Alkaline volcanic rocks from the Columbia Hills, Gusev crater, Mars. *Journal of Geophysical Research*, **111**, E09S91.

Milam, K. A., Stockstill, K. R., Moersch, J. E., et al. (2003) THEMIS characterization of the MER Gusev crater landing site. *Journal of Geophysical Research*, **108**(E12), 8078.

Milliken, R. E., Grotzinger, J. P., and Thomson, B. J. (2010) Paleoclimate of Mars as captured by the stratigraphic record in Gale crater. *Geophysical Research Letters*, **37**. DOI: 10.1029/2009GL041870.

Milliken, R. E., and the MSL Science Team (2014) Mineral mapping of Gale crater using orbital data: results from visible-near infrared reflectance spectroscopy. Available at: www.searchanddiscovery.com/documents/2014/51013milliken/ndx_milliken.pdf.

Ody, A., Poulet, F., Quantin, C., et al. (2015) Candidate source regions of martian meteorites as identified by OMEGA/MEx. *Icarus*, **258**, 366–383.

Parker, M. K., Zegers, T., Kneissi, T., et al. (2010) 3D structure of the Gusev crater region. *Earth and Planetary Science Letters*, **294**, 411–423.

Pelkey, S. M., Jakosky, B. M., and Christensen, P. R. (2004) Surficial properties in Gale crater, Mars, from Mars Odyssey THEMIS data. *Icarus*, **167**, 244–270.

Robbins, S. J., Di Achille, G., and Hynek, B. M. (2011) The volcanic history of Mars: high-resolution crater-based studies of the calderas of 20 volcanoes. *Icarus*, **211**, 1179–1203.

Sautter, V., Fabre, C., Forni, O., et al. (2014) Igneous mineralogy at Bradbury Rise, the first ChemCam campaign at Gale crater. *Journal of Geophysical Research*, **119**, 30–46.

Squyres, S. W., Arvidson, R. E., Blaney, D. W., et al. (2006) The rocks of the Columbia Hills. *Journal of Geophysical Research*, **111**, E02S11.

Squyres, S. W., Aharonson, O., Clark, B. C., et al. (2007) Pyroclastic activity at Home Plate in Gusev crater, Mars. *Science*, **316**, 738–742.

Stolper, E. M., Baker, M. B., Newcombe, M. E., et al. (2013) The petrochemistry of Jake_M: a martian mugearite. *Science*, **341**. DOI: 10.1126/science.1239463.

Tanaka, K. L., Skinner, J. A., Dohm, J. M., et al. (2014) Geologic map of Mars. US Geological Survey Scientific Investigations Map 3292.

Thomson, B. J., Bridges, N. T., Milliken, R., et al. (2011) Constraints on the origin and evolution of the layered mound in Gale crater, Mars using Mars Reconnaissance Orbiter data. *Icarus*, **214**, 413–432.

Tornabene, L. L., Moersch, J. E., McSween, H. Y., et al. (2006) Identification of large (2–10 km) rayed craters on Mars in THEMIS thermal infrared images: implications for possible Martian meteorite source regions. *Journal of Geophysical Research*, **111**, E10006. DOI: 10.1029/2005JE002600.